

# Effect of weld power and build compliance on ultrasonic consolidation

Adam Hehr, Paul J. Wolcott and Marcelo J. Dapino

Department of Mechanical and Aerospace Engineering, The Ohio State University, Columbus, Ohio, USA

## Abstract

**Purpose** – Ultrasonic additive manufacturing (UAM) is a fabrication technology based on ultrasonic metal welding. As a solid-state process, temperatures during UAM fabrication reach a fraction of the melting temperatures of the participating metals. UAM parts can become mechanically compliant during fabrication, which negatively influences the ability of the welder to produce consistent welds. This study aims to evaluate the effect of weld power on weld quality throughout a UAM build, and develop a new power-compensation approach to achieve homogeneous weld quality.

**Design/methodology/approach** – The study utilizes mechanical push-pin testing as a metric of delamination resistance, as well as focused ion beam and scanning electron microscopy to analyze the interface microstructure of UAM parts.

**Findings** – Weld power was found to negatively affect mechanical properties and microstructure. By keeping weld power constant, the delamination energy of UAM coupons was increased 22 per cent along with a consistent grain structure. As a result, to ensure constant properties throughout UAM component construction, maintaining weld power is preferable over the conventional strategy based on amplitude control.

**Research limitations/implications** – Further characterization could be conducted to evaluate the power control strategy on other material combinations, though this study strongly suggests that the proposed approach should work regardless of the metals being welded.

**Practical implications** – The proposed power control strategy can be implemented by monitoring and controlling the electrical power supplied to the welder. As such, no additional hardware is required, making the approach both useful and straightforward to implement.

**Originality/value** – This research paper is the first to recognize and address the negative effect of build compliance on weld power input in UAM. This is also the first paper to correlate measured weld power with the microstructure and mechanical properties of UAM parts.

**Keywords** Welding, Rapid prototyping, Advanced manufacturing technologies, Aluminum, Process innovation

**Paper type** Research paper

## 1. Introduction

Ultrasonic additive manufacturing (UAM), or ultrasonic consolidation, is a recent rapid prototyping process where thin foils of similar or dissimilar metals are ultrasonically welded together in a layer-by-layer process to form gapless, 3D metal parts (Graff, 2011). Along with welding, periodic machining is utilized during the UAM process to fabricate complex features that are not possible with traditional machining processes. Due to the physics of ultrasonic welding, metallic bonding takes place at temperatures far below metallic melting temperatures (Sriraman *et al.*, 2011). Thus, UAM allows temperature-sensitive metals or components to be combined or built into metallic structures. Recently, UAM equipment has been improved by increasing the ultrasonic power nearly an order of magnitude relative to early UAM systems (Graff *et al.*, 2011). This increase in weld power, along with a corresponding increase in available normal force, remedies poor interfacial properties and consolidation quality observed in studies on UAM performed earlier (Kong *et al.*, 2003, 2004; Janaki Ram *et al.*, 2006). The advantage of current

9 kW UAM systems over previous-generation UAM is illustrated in Figure 1. A schematic of a UAM welder and related components is shown in Figure 2.

Ultrasonic metal welding is a solid-state process which works by scrubbing two metals together under pressure at ultrasonic frequencies, which leads to shear of surface asperities, fracture of surface oxides and dispersion of oxides and contaminants away from the weld interface and into the metal matrix. As a consequence of oxide disruption and applied pressure, metallurgically clean surfaces come into close atomic contact and form a metallic bond (Graff *et al.*, 2000). The ultrasonic vibration causes softening or lowering of the metal's yield strength via acoustic softening. Acoustic softening originates from sound energy absorption at dislocations and grain boundaries, producing localized heating and subsequent dislocation motion (Langenecker, 1966). Similar softening can be obtained by bulk heating of the metal. However, bulk heating is less efficient than ultrasonic softening because additional energy is used to heat the entire

The current issue and full text archive of this journal is available on Emerald Insight at: [www.emeraldinsight.com/1355-2546.htm](http://www.emeraldinsight.com/1355-2546.htm)

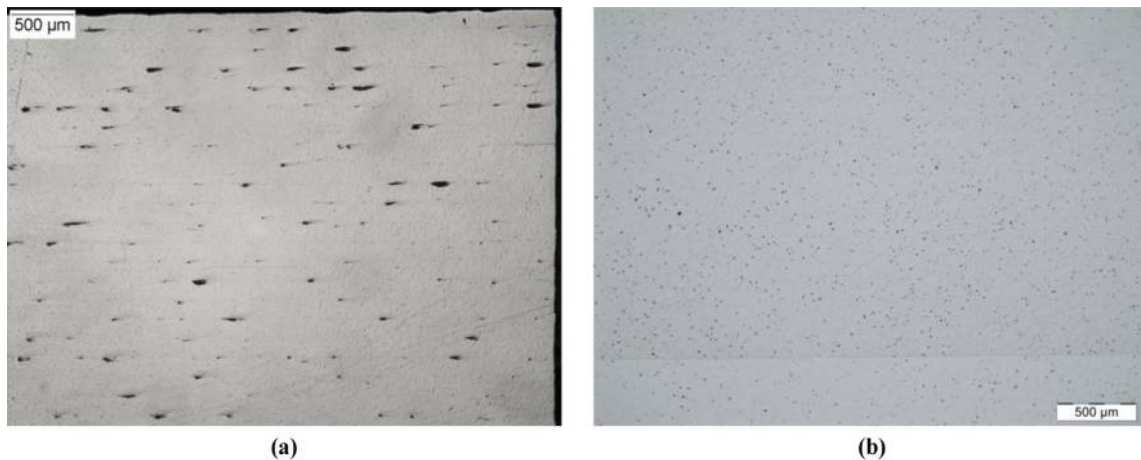


Rapid Prototyping Journal  
22/2 (2016) 377–386  
© Emerald Group Publishing Limited [ISSN 1355-2546]  
[DOI 10.1108/RPJ-11-2014-0147]

Support for A.H. comes from a National Science Foundation Graduate Fellowship, grant No. 1102690. Any opinions, findings and conclusions or recommendations expressed in this material are those of the author(s) and do not necessarily reflect the views of the National Science Foundation. The UAM system utilized in this study was funded by the Ohio Development Services Agency, grant TECH 12-067. The technical assistance of David Tung, Ed Pfeifer and Dan Huber (OSU) is acknowledged.

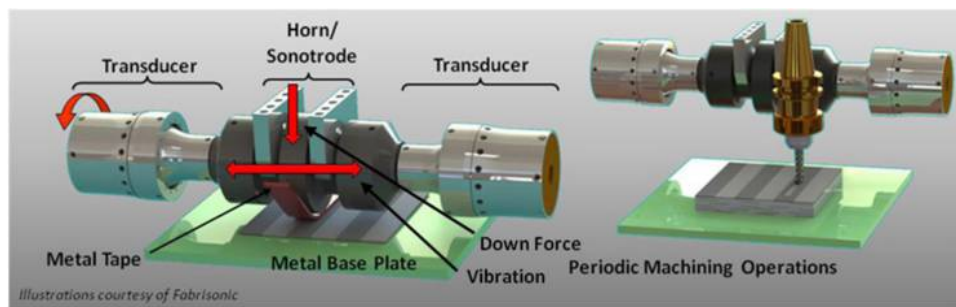
Received 1 November 2014

Accepted 20 January 2015

**Figure 1** Comparison of cross sections of UAM builds

**Notes:** (a) Sample made with first-generation UAM (1 kW of weld power) showing voids along tape interfaces; (b) gapless build made with current UAM equipment (9 kW of weld power)

**Source:** Figure reproduced with permission of Wolcott *et al.* (2014)

**Figure 2** Schematic representation of an ultrasonic additive manufacturing welder (left) and the subtractive CNC stage found in 9 kW UAM systems (right)

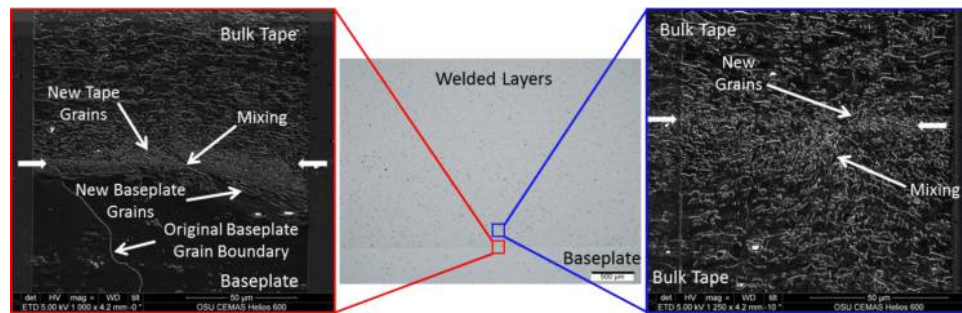
crystal lattice instead of just dislocation dense areas (Langenecker, 1966).

As a consequence of ultrasonic softening lowering a metal's yield stress, large strains can be imparted onto surface asperities near the weld interface without the need for a significant temperature increase. The large strains produce additional dislocation formation (Pal and Stucker, 2013) and plastic deformation heating (Sriraman *et al.*, 2011), creating a kinetic path for dynamic recrystallization, i.e. grain refinement from applied strain and localized heat. The size and statistical distribution of surface asperities influences interface deformation and recrystallization behavior (Truog, 2012; Pal and Stucker, 2013). Observed recrystallized grains from the UAM process are equiaxed and on the order of a micron in size (Johnson, 2008; Dehoff and Babu, 2010), which is similar to other hot working processes where dynamic recrystallization occurs, such as hot rolling and forging (Humphreys and Hatherly, 2004). Figure 3 shows scanning electron microscopy (SEM) images of an ion-beam etched Al 6061-H18 UAM sample with recrystallized grain structure between two tapes and between a tape and an Al 6061-T6 base plate. New grains form near the interface due to large strains imparted from shearing and collapse of asperities.

As in ultrasonic metal welding, the main control variables of UAM include weld speed or time, downforce or pressure between foils and vibration amplitude (assuming a fixed ultrasonic frequency) (Graff *et al.*, 2000). For some materials, a heat plate is utilized to further intensify softening and enhance weldability. However, certain materials like Al 6061 yield quality welds with no additional heating, as sufficient weld energy is available from 9 kW UAM welders (Wolcott *et al.*, 2014). The input weld energy can be expressed as a function of the main control variables by assuming energy is imparted into the structure through mechanical scrubbing or mechanical power, expressed as:

$$E_{\text{weld}} = \int P \cdot dt = \int F \cdot V_w \cdot dt = \frac{1}{V_t} \int F \cdot \omega \cdot \delta \cdot dx. \quad (1)$$

Here,  $F$  is the scrubbing or shear force at the interface, which is a function of the downforce during initial tape slip (due to sliding friction) and of the vibration amplitude of the sonotrode after slip ceases (due to shear deformation during collapse of asperities). The variable  $V_w$  is the velocity of the sonotrode vibration, or the derivative of the vibration displacement  $\delta$  and  $\omega$  is the fixed frequency at which the

**Figure 3** Al 6061-H18 sample showing a recrystallized grain structure between two tapes and between a tape and the 6061-T6 base plate

**Notes:** Tape-to-tape boundaries cannot be optically identified due to full collapse of interface asperities and absence of voids. New grains originate at the interface from large shear strains in asperities and localized interface heating. The sample was imaged on an SEM after it was etched with a dual focused ion beam

welder vibrates. The welder displacement and velocity are both sinusoidal functions. The integral (1) is calculated over the amount of time the welder is welding a specific tape area, based on the weld speed  $V_f$  at which the welder rolls along the surface of the structure.

It is emphasized that energy conversion takes place from electrical to mechanical energy in the piezoelectric transducers. As a result, the input weld energy can be indirectly measured in practice by measuring the applied electrical current and voltage to the transducers and from knowledge of the electrical to mechanical energy transfer efficiency of the piezoelectric transducers. The efficiency has been estimated to range between 80 and 90 per cent (Graff *et al.*, 2000). Deformation and recrystallization have been observed in the bulk tape (though in smaller quantities than in the interface), suggesting that not all weld energy is transmitted and stored at the interface (Fujii *et al.*, 2011; Sojiphan *et al.*, 2011).

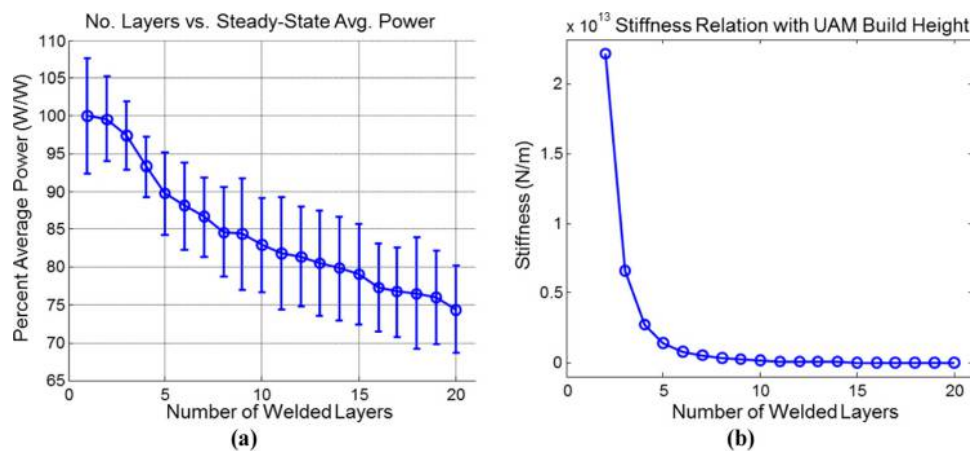
It has been shown that high vibration amplitudes and slow speeds lead to relatively higher temperature generation during the UAM process (Sriraman *et al.*, 2011) and higher

out-of-plane delamination resistance in UAM builds (Wolcott *et al.*, 2014). These results show that:

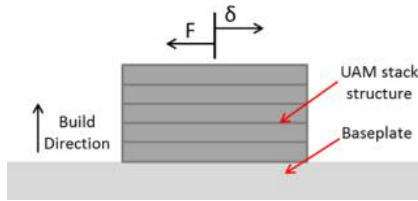
- mechanical energy is converted into both thermal and strain energy; and
- that energy is stored within the build's microstructure from the welding operation.

Because the UAM process entails building a structural component which has a finite mechanical compliance, the available weld energy can be negatively affected by the structure itself. Build compliance can lead to inconsistent weld quality during build construction (Gibert *et al.*, 2010) and inconsistent interface recrystallization behavior as a function of build height (Fujii *et al.*, 2011; Sojiphan *et al.*, 2012). An example of how compliance negatively affects weld energy is shown in Figure 4(a), where measurements of the average ultrasonic power were taken at various layers through the height of a UAM build. This UAM build is shown schematically in Figure 5.

Figure 4(a) shows that the weld input power decays exponentially as a function of build height. The drop in weld

**Figure 4** Effect of build compliance on weld input power for a stack of welded Al foils

**Notes:** (a) Measured average power over steady-state weld zone with one standard deviation error bars; (b) build stiffness as a function of layer number

**Figure 5** UAM stack schematic showing vibration amplitude,  $\delta$  and reaction force,  $F$ 

input power occurs because the build's reaction force to the scrubbing or shear force produced by the sonotrode decreases due to compliance added by each layer. Because the UAM build behaves like a cantilever beam, its stiffness can be expressed as:

$$k = \frac{3EI}{(Nt)^3}. \quad (2)$$

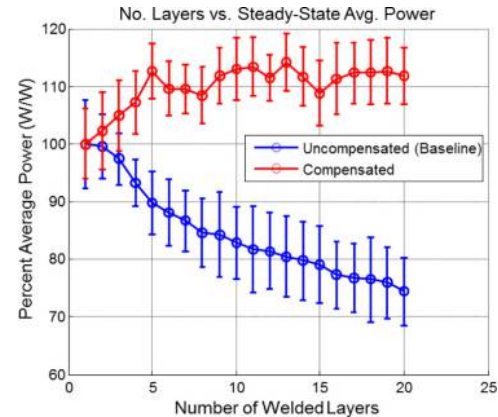
Here,  $E$  is the modulus of elasticity,  $I$  is the second moment of inertia,  $N$  denotes the number of layers and  $t$  represents the foil thickness. The stiffness is plotted as a function of welded layers in Figure 4(b).

Figure 4 shows correlation between the two plots because energy input into the build is a function of the build's stiffness and sonotrode displacement. The energy input can be modeled using the definition of mechanical work and the beam stiffness:

$$Work = \int F \cdot d\delta = \frac{1}{2} \frac{3EI}{(Nt)^3} \delta^2. \quad (3)$$

The force is assumed to be equal and opposite to the reaction force from the sonotrode (Figure 5). The work or energy input decreases with build height if the vibration amplitude remains constant throughout the build process. The purpose of the cantilever stiffness expression (2) and work expression (3) is to qualitatively show that compliance has an impact on measured ultrasonic transducer power draw. In reality, large plastic strains occur during welding, making the linear compliance assumption inaccurate for quantitatively describing the energy loss due to compliance. To maintain constant weld energy or power throughout the build's height, an amplitude compensation approach is necessary. Table I shows the amplitude compensation applied experimentally to the end of the UAM stack.

As shown in Figure 6, power loss can be effectively compensated by adjusting the amplitude of vibration of the sonotrode. Consequently, the purpose of this study is to investigate the effect of weld input power on the properties of UAM builds, and demonstrate that power-compensated UAM produces more consistent builds than amplitude compensation. The latter approach is typical of current UAM

**Figure 6** Measured power without and with amplitude compensation

**Notes:** The compensated build maintains the power applied to the build within +15 per cent, whereas the uncompensated build shows a decay in input power of 25 per cent by the 20th layer

systems. In particular, bulk delamination resistance testing was carried out using push-pin testing, and the interfacial microstructure was evaluated using focused ion beam (FIB) imaging and SEM.

## 2. Experimental methods

### 2.1 Sample manufacturing

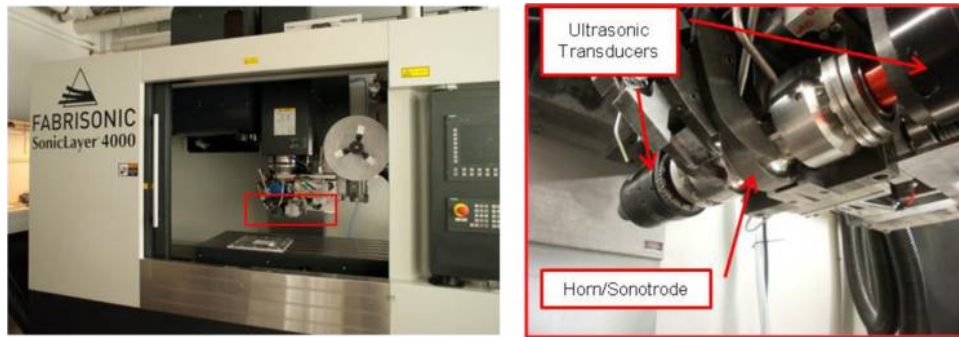
In this study, aluminum 6061-H18[1] was utilized for fabrication and testing. Aluminum 6061 was chosen due to its frequent use in industry and strong compatibility with UAM. Push-pin samples were manufactured on a 9 kW UAM system, shown in Figure 7. This machine is fully automated, includes computer numerical control (CNC) and laser machining capabilities to complement the additive ultrasonic welding stage, and allows the user to record ultrasonic transducer power profiles during welding.

Welding was performed with a 7- $\mu\text{m}$   $R_a$  surface roughness sonotrode on a 1.27 cm-(0.5 in)-thick aluminum 6061-T6 base plate. The base plate was constrained with a vacuum chuck while two 2.54 cm-(1 in)-wide, 0.152 mm-(0.006 in)-thick and 30.5 cm-(12 in)-long strips of foil were welded sequentially onto each other to create two stacks (Figure 8). Each stack is 20 layers-high, yielding four push-pin samples cut using the integrated CNC stage. One stack was manufactured without power compensation, i.e. a constant amplitude of 32.76  $\mu\text{m}$  was used on all the layers. The other stack was fabricated by manually altering amplitude levels (Table I) to keep the weld power input constant throughout the thickness of the stack. Other welding variables were held constant, as summarized in Table II.

**Table I** Power compensation approach by changing amplitude per layer

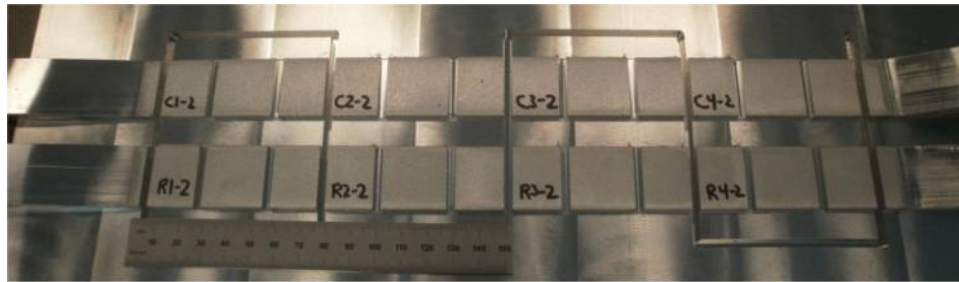
Layer	1-2	3	4	5	6	7-8	9	10-12	13-15	16-20
Amplitude (%)	70	72	74	76	76	77	78	78	79	80
Amplitude ( $\mu\text{m}$ )	32.7	33.6	34.6	35.5	35.5	36.0	36.4	36.4	36.9	37.4

**Figure 7** Fabrisonic's 9 kW SonicLayer™ 4000 UAM system utilized to fabricate samples in this study



**Source:** Figure slightly modified and reproduced with permission of Wolcott *et al.* (2014)

**Figure 8** Push-pin samples constructed with 9 kW UAM system and integrated CNC milling stage



**Note:** In the image, C stands for compensated, while R stands for reference, i.e. uncompensated

**Table II** Control variables utilized for welding samples

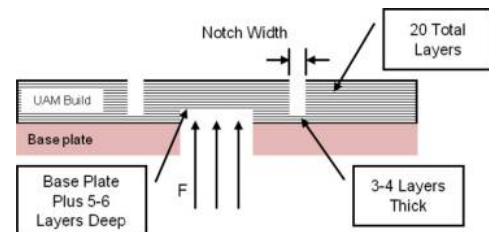
Temperature	22°C (72°F)
Weld Force	5,000 N
Amplitude	32.76–37.4 $\mu\text{m}$ (70–80%)
Weld Speed	84.6 mm/sec (200 in/min)

During the construction of the stacks, power profiles were measured for layers 2, 5, 10, 15 and 20. The profiles were recorded using the diagnostics tab of the UAM system's Siemens controller and were subsequently output to MS Excel and MATLAB for analysis. After welding, machining was performed to final sample dimensions using the built-in machining center, a band saw and a manual three-axis mill.

## 2.2 Mechanical testing

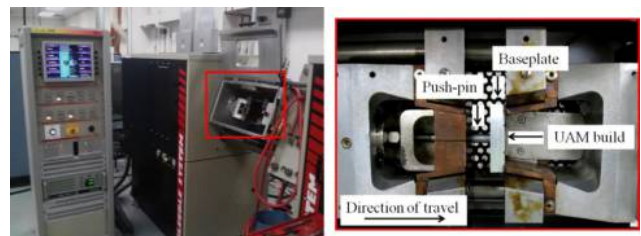
The push-pin test and associated sample design, as originally proposed by Zhang *et al.* (2009), has been utilized for UAM bond assessment (Truog, 2012; Wolcott *et al.*, 2014). Push-pin testing provides a measure of delamination resistance through multiple layers, with failure driven by both shear and tensile stress components (Zhang *et al.*, 2009). Because push-pin specimens require few layers, the method is both effective (for comparison purposes) and efficient. A schematic of the sample geometry is presented in Figure 9, while the test equipment is shown in Figure 10. Sample testing was performed using a Gleeble™ thermal-mechanical simulator; this machine's test time is short, and it has high

**Figure 9** Schematic of push-pin sample design utilized in this study



**Source:** Figure slightly modified and reproduced with permission of Wolcott *et al.* (2014)

**Figure 10** Gleeble™ thermal-mechanical tester utilized for push-pin testing with key test details shown in the inset



**Source:** Figure reproduced with permission of Wolcott *et al.* (2014)

stiffness to minimize deformation estimate errors. The push-out rate was set to 12 mm/min, while samples were manually positioned close to the mechanical stop prior to loading. Manual positioning was done because test time could be significantly reduced, yet the sample distance from the mechanical stop was not consistent throughout testing. Consequently, samples did not begin to take on load at the same distance for each test. However, the variation in starting distance has no consequence on test results. Both force and distance were recorded.

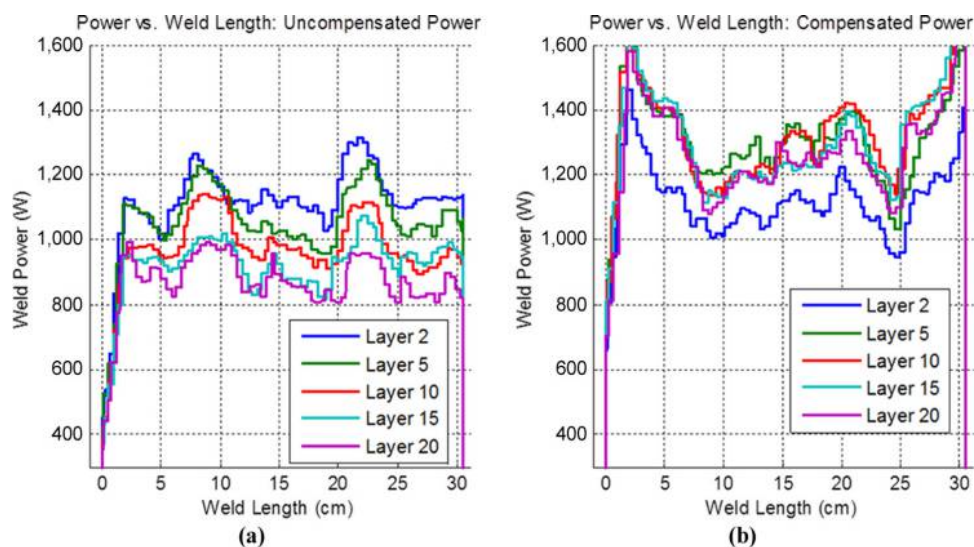
### 2.3 Microstructure evaluation

Along with mechanical testing, microstructure imaging was carried out to qualitatively and quantitatively characterize recrystallization behavior at key weld interfaces. FIB imaging was utilized to expose grains in specific areas, while concurrent SEM was used to image the microstructure. The equipment utilized was a FEI Helios NanoLab<sup>TM</sup> 600 DualBeam FIB/SEM (Cemas.osu.edu, 2014). Ion beam etching works in a similar manner to chemical etchants by exposing grain-to-grain contrast via grain orientation, yet with a more controlled material removal than chemical etchants. FIB etching was carried out using an oblique incident angle with an accelerating voltage of 30 keV, while SEM imaging utilized an acceleration voltage of 5 keV and a working distance of approximately 4.2 mm.

## 3. Experimental results

Weld power profiles measured during sample construction are provided in Figure 11 for both uncompensated and compensated builds. The weld power is shown for layers 2, 5, 10, 15 and 20. In all cases, especially after the second layer, the average power delivered to the part is higher and more consistent in the power control mode [Figure 11(b)] than the amplitude control mode [Figure 11(a)]. The power profiles show variation around a mean value along the weld length, after a transient region at the onset of the weld.

**Figure 11** Measured power curves during push-pin sample construction



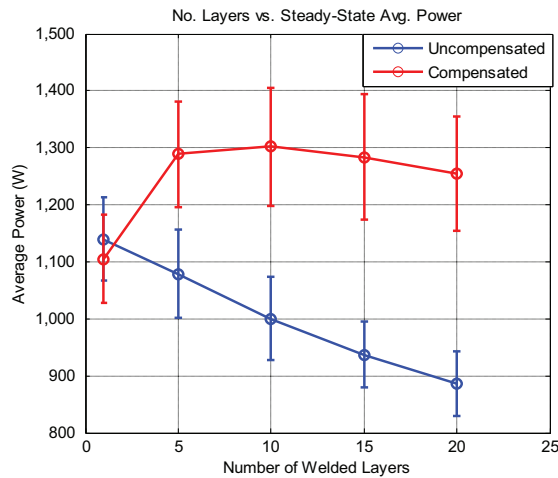
**Notes:** (a) Uncompensated build; (b) compensated build

Average power was calculated by averaging instantaneous power between 2.5 cm and 28 cm for the measurements shown in Figure 11. Power was calculated without the start and end of the weld to avoid transient behavior and to obtain a more representative steady-state calculation of the process. The calculated power average is shown in Figure 12, with error bars representing the first standard deviation of the instantaneous power signal. Figure 12 shows power decay for the uncompensated build of 23 per cent over 20 layers, while the compensated build shows nearly constant power after layer 5. These trends are similar to those seen in preliminary studies (Figure 6).

Representative push-pin test data are shown in Figure 13, while total test statistics are presented in Table III. The samples built with compensated power exhibit failure through all the welded layers compared to the uncompensated samples. Additionally, the compensated samples require additional mechanical work to drive the sample to failure and exhibit slightly higher strength.

Typical microstructure analysis for the 5th and 15th tape interfaces for the uncompensated and compensated power samples is shown in Figure 14. Interfaces 5 and 15 were chosen for comparison because push-pin testing occurs near layer 5 and above. The compensated power samples had nearly identical power inputs at these interfaces, and uncompensated power samples were subjected to a significantly different power input. The cross sections were cut near 15 cm of weld length to avoid transient regions and to use a region representative of the average weld power (Figure 11). Figure 14 shows fine grains at all the interfaces. However, for the 15th uncompensated power weld interface, the recrystallized region is narrow, showing little to no mixing in some areas. On the other hand, the 15th compensated power interface shows strong mixing character and dimensions similar to the 5th power-compensated interface.

**Figure 12** Average weld power as a function of number of welded layers, both for uncompensated and compensated builds



**Notes:** The trends are similar to the measurements shown in figure 5

#### 4. Discussion

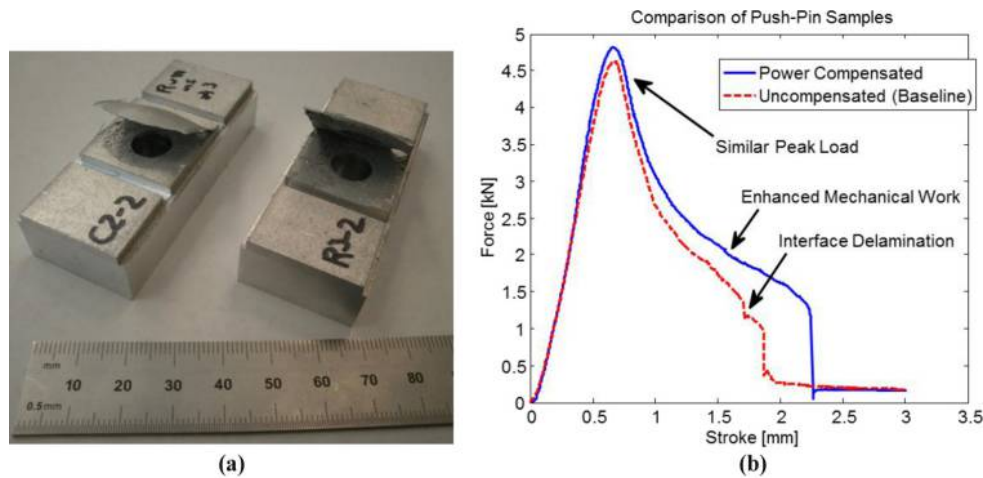
The hypothesis of structural compliance impacting ultrasonic weld power and corresponding mechanical strength and microstructure was tested in this study. A “compliant” UAM

stack structure was constructed with the existing amplitude control framework, while another stack was made by varying the amplitude to counteract stiffness loss and maintain constant weld power during the build process. Amplitude compensation provides the framework for constant weld power as a function of stack height. Mechanical push-pin testing and microstructure analysis were conducted to evaluate weld bond strength and weld microstructure, respectively.

Push-pin testing has proven to be a good indicator of weld quality (Wolcott *et al.*, 2014), especially in comparative studies such as the one presented here. The tests were conducted on material between the 5th and 20th interfaces due to sample design requiring testing away from the base plate interface (Figure 9). As a result, there is no contribution from lower layers. As shown in Table III, push-pin results show that the power-compensated stack requires on average higher mechanical push-out energy while exhibiting improved failure behavior (Figure 13). Compensated samples show nearly 22 per cent more push-out energy over uncompensated samples. As a result, energy is being stored within the sample during construction due to higher power inputs leading to higher push-out energy.

To investigate this internal energy storage in more detail, microstructure analysis was conducted with the use of FIB and SEM imaging. It was found that the compensated sample’s 5th and 15th interface microstructures were very

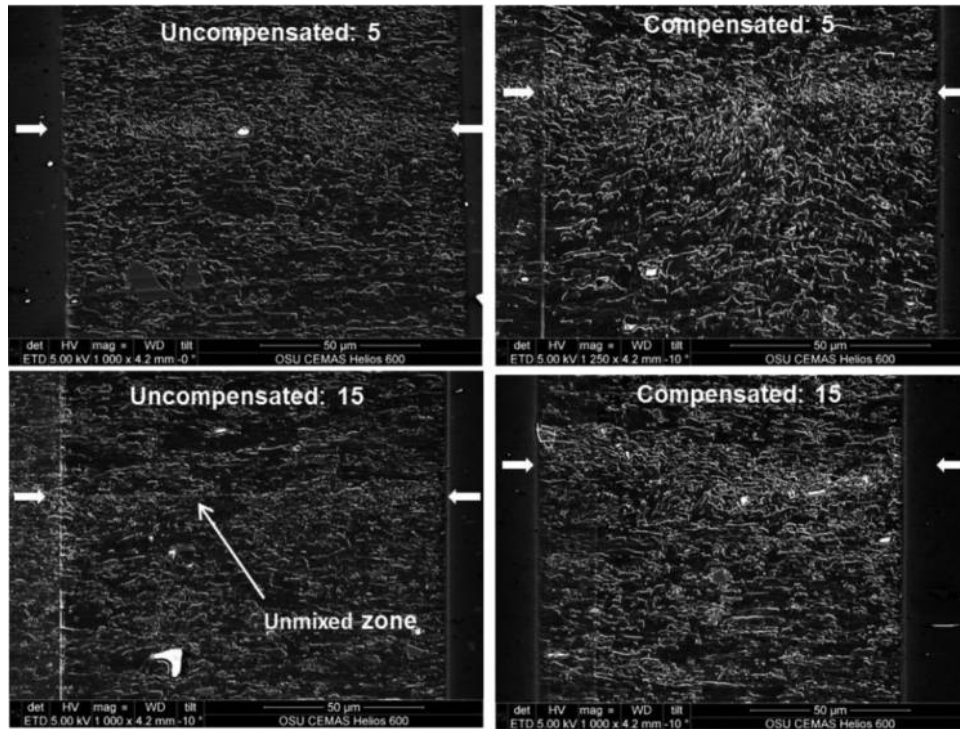
**Figure 13** Comparison between compensated and uncompensated push-pin samples



**Notes:** (a) Photo comparing failure behavior; (b) force-displacement plots

**Table III** Complete statistics for uncompensated and compensated push-pin samples

Sample	Uncompensated		Compensated	
	Peak force (kN)	Push-out energy (kN × mm)	Peak force (kN)	Push-out energy (kN × mm)
1	4.72	3.64	5.02	5.40
2	4.67	4.78	4.83	5.53
3	4.66	4.63	5.20	6.19
4	4.25	4.81	4.50	4.75
Mean	4.58	4.47	4.89	5.47
SD	0.19	0.48	0.26	0.51

**Figure 14** Interface microstructure at layers 5 and 15 for uncompensated and compensated samples

**Notes:** Samples were sectioned and polished for analysis near 15 cm of weld length to avoid transient weld regions. Arrows have been added to indicate the approximate interface region. Grain refinement can be seen at the interface regions as expected, yet poor mixing and less grain refinement are observed at the uncompensated 15th layer, while the compensated 15th layer is like the uncompensated 5th layer. The difference in mixing and grain refinement originates from the uncompensated sample having received less strain energy.

similar in size and character, which supports the fact that these two interfaces were welded with similar power levels (Figure 12). On the other hand, the uncompensated sample's recrystallized interfaces were inconsistent in mixing character and in size due to less imparted strain energy during welding. This result is sensible considering that the weld power input differed by 18 per cent between the layers. New small grains are a measure of stored energy because grain boundaries have an associated energy (Abbaschian *et al.*, 2010). Consequently, the presence of many small grains implies increased energy storage due to an increase in net grain boundary area. According to the Hall–Petch relationship, high volumes of small grains lead to improved mechanical properties, which in turn supports why improved mechanical properties are observed with power-compensated builds over uncompensated builds. This energy conversion from weld input to microstructure storage can be expressed with the proposed energy balance:

$$E_{surf} + E_{weld} = E_{bulk} + E_{recryst} + E_{thermal} \quad (4)$$

where  $E_{surf}$  is the combined surface energy of the surface to weld onto and the surface of the tape which will soon be welded. This is a constant empirical parameter because surfaces are not altered prior to welding and assumed to be constant.  $E_{weld}$  is the imparted weld energy onto the two

surfaces, a function of processing variables as described earlier (equation 1); this parameter can be indirectly measured with transducer power draw.  $E_{bulk}$  is the energy corresponding to the joined surfaces, solely. This energy is a function of oxide dispersal and bond quality, which is influenced by  $E_{weld}$ .  $E_{recryst}$  is the energy corresponding to the volume of material near the interface which undergoes recrystallization, i.e. nucleation of new grains. It can be quantified by measuring the volume of material which has new grains.  $E_{recryst}$  is a function of both strain energy and temperature.  $E_{thermal}$  is the thermal energy which does not contribute to kinetic recrystallization and is waste.

Other researchers have also utilized energy principles to model the UAM process (Kong *et al.*, 2005; Yang *et al.*, 2010; Kelly *et al.*, 2014). However, their formulations do not utilize empirical weld power to validate their method and do not consider microstructure effects. Instead, they fit physics-based models to peel strength and linear weld density correlations. Others have modeled the UAM process with sophisticated finite element modeling techniques which theorize frictional heating (de Vries, 2004; Zhang and Li, 2008; Siddiq and Ghassemieh, 2009), vacancy motion (Yadav and Doumanidis, 2005), acoustic softening (Kelly *et al.*, 2013) and dislocation accumulation (Pal and Stucker, 2013) as the primary bonding mechanism. However, these models are complex, have many

fitting parameters and do not have strong empirical evidence to support in-situ estimation of bond quality. In-situ bond tracking has been carried out using a photonic Doppler velocimeter (Foster *et al.*, 2014), yet significant development is required to correlate velocity behavior with bond quality, expensive equipment is required for the technique and focusing on components of concern is difficult due to small tape thickness.

## 5. Concluding remarks

The hypothesis of structural compliance impacting ultrasonic weld power and corresponding mechanical strength and microstructure was tested in this study and found to be influential. It was shown that both mechanical testing and microstructure analysis correlate with variations in weld power input due to poor properties being observed when power was not held constant through the UAM process. Consequently, future UAM systems should incorporate means to monitor and control weld power during the UAM process to improve component quality and identify defects arising from dramatic stiffness loss. This proposed in-situ weld power monitoring approach does not require additional equipment and shows strong promise to estimate bond quality for design and quality tracking purposes.

Although amplitude control has shown to be vulnerable to the negative effect of structural compliance, the variable still has merit because it originally defines the required power input to produce a strong weld. Thus, it may be beneficial to initially use amplitude control to provide a baseline power level, and then maintain that weld power throughout the build process.

Finally, evidence presented in this study plausibly confirms the hypothesis of energy storage within the microstructure considering the comparative nature of the push-pin test and small fraction of investigated microstructure. A more rigorous investigation of out-of-plane tensile testing and microstructure examination is required for full validation. Future microstructure analysis will require additional samples and electron backscatter diffraction to more completely understand how energy is transferred to the interface and bulk tape.

## Note

- 1 Al 6061-H18 foil was fabricated by work hardening annealed Al 6061 through a H18 process.

## References

- Abbaschian, R., Abbaschian, L. and Reed-Hill, R.E. (2010), *Physical Metallurgy Principles*, Cengage Learning, Stamford.
- Cemas.osu.edu (2014), *Center for Electron Microscopy and Analysis (GEMAS)*, available at: <http://cemas.osu.edu/> (accessed 30 September 2014).
- de Vries, D. (2004), "Mechanics and mechanisms of ultrasonic metal welding", PhD thesis, The Ohio State University, Columbus, OH.
- Dehoff, R. and Babu, S. (2010), "Characterization of interfacial microstructures in 3003 aluminum alloy blocks fabricated by ultrasonic additive manufacturing", *Acta Materialia*, Vol. 58, pp. 4305–4315.
- Foster, D., Taber, G., Babu, S. and Daehn, G. (2014), "In situ velocity measurements of very high power ultrasonic additive manufacturing using a photonic Doppler velocimeter", *Science and Technology of Welding and Joining*, Vol. 19 No. 2, pp. 157–163.
- Fujii, H.T., Sriraman, M.R., Babu, S.S. (2011), "Quantitative evaluation of bulk and interface microstructures in Al-3003 alloy builds made by very high power ultrasonic additive manufacturing", *Metallurgical and Materials Transactions A*, Vol. 42 No. 13, pp. 4045–4055.
- Gibert, J., Austin, E. and Fadel, G. (2010), "Effect of height to width ratio on the dynamics of ultrasonic consolidation", *Rapid Prototyping Journal*, Vol. 16 No. 4, pp. 284–294.
- Graff, K. (2011), "Ultrasonic additive manufacturing", *ASM Handbooks: Volume 6A, Welding Fundamentals and Processes*, American Society for Materials International, Materials Park, OH.
- Graff, K., Devine, J., Keltos, J. and Zhou, N. (2000), "Ultrasonic welding of metals", *American Welding Society Welding Handbook*, American Welding Society, Miami, FL.
- Graff, K., Short, M. and Norfolk, M. (2011), *Very High Power Ultrasonic Additive Manufacturing (VHP UAM)*, Edison Welding Institute, Columbus, OH.
- Humphreys, F. and Hatherly, M. (2004), *Recrystallization and Related Annealing Phenomena*, Elsevier.
- Janaki Ram, G.D., Yang, Y., Stucker, B.E. (2006), "Effect of process parameters on bond formation during ultrasonic consolidation of aluminum alloy 3003", *Journal of Manufacturing Systems*, Vol. 25 No. 3, pp. 221–238.
- Johnson, K. (2008), "Interlaminar subgrain refinement in ultrasonic consolidation", PhD thesis, Loughborough University.
- Kelly, G., Advania, S., Gillespie, J. and Bogetti, T. (2013), "A model to characterize acoustic softening during ultrasonic consolidation", *Journal of Materials Processing Technology*, Vol. 213, pp. 1835–1845.
- Kelly, G., Just, M., Advani, S. and Gillespie, J. (2014), "Energy and bond strength development during ultrasonic consolidation", *Journal of Materials Processing Technology*, Vol. 214, pp. 1665–1672.
- Kong, C., Soar, R. and Dickens, P. (2003), "Characterisation of aluminium alloy 6061 for the ultrasonic consolidation process", *Materials Science and Engineering A*, Vol. 363 Nos 1/2, pp. 99–106.
- Kong, C., Soar, R. and Dickens, P. (2004), "Optimum process parameters for ultrasonic consolidation of 3003 aluminium", *Journal of Materials Processing Technology*, Vol. 146 No. 2, pp. 181–187.
- Kong, C.Y., Soar, R. and Dickens, P. (2005), "A model for weld strength in ultrasonically consolidated components", *Journal of Mechanical Engineering Science*, Vol. 219 No. 1, pp. 83–91.
- Langenecker, B. (1966), "Effects of ultrasound on deformation characteristics of metals", *IEEE Transactions Sonics and Ultrasonics*, Vol. 13 No. 1.
- Pal, D. and Stucker, B. (2013), "A study of subgrain formation in Al 3003 H-18 foils undergoing ultrasonic additive manufacturing using a dislocation density based crystal plasticity finite element framework", *Journal of Applied Physics*, Vol. 113.

- Siddiq, A. and Ghassemieh, E. (2009), "Theoretical and FE analysis of ultrasonic welding of aluminum alloy 3003", *Journal of Manufacturing Science and Engineering*, Vol. 131 No. 4.
- Sojiphan, K., Babu, S.S., Yu, X., Vogel, S.C. (2012), "Quantitative evaluation of crystallographic texture in aluminum alloy builds fabricated by very high power ultrasonic additive manufacturing", *Proceedings of the International Solid Freeform Fabrication Symposium 2012, Austin, TX*, pp. 364-372.
- Sojiphan, K., Sriraman, M.R., Babu, S.S. (2011), "Stability of microstructure in Al3003 builds made by very high power ultrasonic additive manufacturing", *Proceedings of Materials Science and Technology 2011 Conference and Exhibition, Columbus, OH*, pp. 362-371.
- Sriraman, M.R., Gonser, M., Fujii, H.T., Babu, S.S. and Bloss, M. (2011), "Thermal transients during processing of materials by very high power ultrasonic additive manufacturing", *Journal of Materials Processing Technology*, Vol. 211 No. 10, pp. 1650-1657.
- Truog, A.G. (2012), "Bond improvement of Al/Cu joints created by very high power ultrasonic additive manufacturing", Master's thesis, OSU Welding Department, Columbus.
- Wolcott, P., Hehr, A. and Dapino, M.J. (2014), "Optimized welding parameters of Al 6061 ultrasonic additive manufactured structures", *Journal of Materials Research*, Vol. 29 No. 18.
- Yadav, S. and Doumanidis, C. (2005), "Thermomechanical analysis of an ultrasonic rapid manufacturing (URM) system", *Journal of Manufacturing Processes*, Vol. 7 No. 2.
- Yang, Y., Ram, G. and Stucker, B. (2010), "An analytical energy model for metal foil deposition in ultrasonic consolidation", *Rapid Prototyping Journal*, Vol. 16 No. 1, pp. 20-28.
- Zhang, C., Deceuster, A. and Li, L. (2009), "A Method for bond strength evaluation for laminated structures with application to ultrasonic consolidation", *Journal of Materials Engineering and Performance*, Vol. 18 No. 8, pp. 1124-1132.

- Zhang, C. and Li, L. (2008), "A friction-based finite element analysis of ultrasonic consolidation", *Welding Journal*, Vol. 87 No. 7, pp. 187-194.

### About the authors

**Adam Hehr** is a PhD student under the guidance of Professor Marcelo J. Dapino in OSU's Smart Materials and Structures Lab ([www.mecheng.osu.edu/smsl/](http://www.mecheng.osu.edu/smsl/)). His research interests are focused on UAM applications, UAM improvement, dissimilar metal joining, structural health monitoring, sensors, composites and smart materials. Adam is a National Science Foundation Graduate Research Fellow ([www.nsfgrfp.org/](http://www.nsfgrfp.org/)) who obtained his bachelor's and master's degrees from the University of Cincinnati.

**Paul J. Wolcott** is a PhD student in the Department of Mechanical Engineering at The Ohio State University, where he is a member of the Smart Materials and Structures Laboratory. He completed his bachelor's degree in the Department of Materials Science and Engineering at The University of Michigan and before joining OSU, he worked at General Motors conducting research and development for advanced fuel cell vehicles. He has completed his master's degree in mechanical engineering at OSU investigating the fundamentals of ultrasonic additive manufacturing applied to both passive and active materials, which is also the focus of his PhD work.

**Marcelo J. Dapino**, PhD, is The Honda R&D Americas Designated Chair in Engineering at The Ohio State University, where he is a Mechanical Engineering Professor. He serves as Director of the Honda-OSU Mobility Innovation Exchange (MIX), a major collaborative program of sponsored research and education bridging the two organizations, and is Associate Director for Research of the Smart Vehicle Concepts Center, a National Science Foundation Industry/University Collaborative Research Center. As author of over 160 technical articles, Professor Dapino is an internationally recognized leader in the areas of design, manufacturing, dynamics and control of smart materials. Professor Dapino is a Fellow of ASME. Marcelo J. Dapino is the corresponding author and can be contacted at: [dapino.1@osu.edu](mailto:dapino.1@osu.edu)

**This article has been cited by:**

1. Adam Hehr, Justin Wenning, Kurt Terrani, Sudarsanam Suresh Babu, Mark Norfolk. 2017. Five-Axis Ultrasonic Additive Manufacturing for Nuclear Component Manufacture. *JOM* **69**:3, 485-490. [[CrossRef](#)]
2. Adam Hehr, Marcelo J. Dapino. 2017. Dynamics of ultrasonic additive manufacturing. *Ultrasonics* **73**, 49-66. [[CrossRef](#)]
3. P.J. Wolcott, A. Hehr, C. Pawlowski, M.J. Dapino. 2016. Process improvements and characterization of ultrasonic additive manufactured structures. *Journal of Materials Processing Technology* **233**, 44-52. [[CrossRef](#)]